ARTICLE

Comparison of CH, C_3, CHF, and CF_2 Surface Reactivities during Plasma-Enhanced Chemical Vapor Deposition of Fluorocarbon Films

Dongping Liu, Michael F. Cuddy, and Ellen R. Fisher*

Department of Chemistry, Colorado State University, Fort Collins, Colorado 80523-1872

ABSTRACT The overall character of films deposited using plasma-enhanced chemical vapor deposition relies on the interactions of gas-phase molecules with the depositing film surface. The steady-state surface interactions of CH, C_3, CHF, and CF_2 have been characterized at the interface of depositing fluorocarbon (FC) films using the imaging of radicals interacting with surfaces (IRIS) technique. IRIS measurements show that the relative gas-phase densities of CH, C_3, CHF, and CF_2 in mixed FC plasmas depend on the CH_2F_2/C_3F_8 ratio. Similar results are found using optical emission spectroscopy to monitor the production of excited-state plasma species. The effects of plasma parameters, such as the feed gas composition and substrate bias on the radical surface, were measured. Under all conditions, the surface reactivity for CH radicals is near unity, whereas those for C_3, CHF, and CF_2 exhibit very low surface reactivity but also show some dependence on experimental parameters. Under some conditions, CF_2 and CHF are generated at the surface of the depositing film. Surface reactivity measurements indicate that CF_2, CHF, and C_3 may contribute to FC growth only when adsorbing at reactive sites at the film surface. Moreover, the low surface reactivities of singlet species such as C_3, CF_2, and CHF may be related to the electronic configuration of the molecules.

KEYWORDS: surface interactions • plasma modification • fluorocarbon polymers • laser-induced fluorescence • optical emission spectroscopy

I. INTRODUCTION

Ultralarge-scale integrated circuits (ULSIs) have been used extensively in the microelectronics industry, and the development of alternative low dielectric constant materials for interlayer dielectrics has become a topic of intense interest. Materials with low dielectric constants are used to reduce the capacitance of dielectric interlayers and improve the signal processing performance in ULSIs (1, 2). Fluorocarbon (FC) films synthesized by plasma-enhanced chemical vapor deposition (PECVD) are good candidates for such dielectric materials because they have a relatively low dielectric constant of less than 2.0 (1, 3). FC films with low dielectric constants have been successfully deposited using various FC gases such as CF_4 (4), C_2F_6 (4, 5), C_3F_8 (6), C_4F_8 (6, 7), C_3F_6O (8−10), CH_2F_2 (11), $C_2H_2F_4$ (11, 12), and CHF_3 (13). In addition to the deposition of FC films, FC plasmas are also of interest for selective etching of hard masks such as Si_3N_4 over new photoresists used in 193 nm ArF photolithography processes (14). In these systems, mixtures of two FC gases (e.g., CHF_3/CF_4) and/or mixtures of FC gases and H_2 (e.g., CH_2F_2/H_2) are used to maximize etch selectivity while minimizing unwanted FC deposits.

* Author to whom correspondence should be addressed. E-mail: erfisher@lamar.colostate.edu.
Received for review January 15, 2009 and accepted March 12, 2009

DOI: 10.1021/am900034x
© 2009 American Chemical Society

In an examination of films deposited in FC plasmas, high-resolution C 1s X-ray photoelectron spectroscopy (XPS) data reveal that a complex carbon-binding environment can be created via the PECVD process. Comparable concentrations of CF_3, CF_2, CF, and quaternary carbon moieties can be found in many FC materials deposited via PECVD (15). The ability to control the structure of deposited materials is critical because the low dielectric constants (3), hydrophobicity (16), and dangling bond density of FC films (17, 18) are associated with their structures. Previous results from our group demonstrated that high-CF_2-content films can be achieved via downstream and pulsed PECVD using hexafluoropropylene oxide (HFPO) as well as C_3F_8 precursors (9, 10). Other plasma parameters such as applied power, pressure, and feed gas ratios strongly influence the resulting film chemistry (14, 15, 19).

Not surprisingly, neutral plasma species are thought to play essential roles in achieving the desired material properties and etch rates (20). A basic understanding of the fundamental processes that occur in FC plasmas is essential in optimizing the performance of these systems. Thus, considerable effort has been focused on investigating the role of CF_x ($x = 1-3$) molecules in both deposition and etching FC plasmas, especially at the gas−surface interface. Several techniques have been employed to examine CF_x species, including infrared laser absorption spectroscopy (21), threshold ionization mass spectroscopy (22, 23), and laser-induced fluorescence (LIF) spectroscopy (24, 25). These studies have primarily focused on the gas-phase densities

Published on Web 04/03/2009

of various species as a function of the plasma parameters and attempts to correlate these densities with the resulting film properties have been somewhat limited. We have previously used our imaging of radicals interacting with surfaces (IRIS) technique, which employs LIF for detection of plasma species, to measure the CF_2 surface reactivity using depositing FC plasmas (5, 6, 13, 26−28). Results indicate that CF_2 may contribute to the FC film growth only when adsorbing at radical sites created at the film surface. More importantly, results from a range of FC precursors demonstrated that energetic ion bombardment of the deposited FC film results in the surface production of CF_2 under a range of conditions. The investigation of CF_x radicals is not, however, sufficient to understand the overall reaction kinetics in FC plasmas and FC film deposition processes. Several other radicals likely participate in gas-phase and surface reactions during film deposition, especially in systems that involve multiple gases as precursors.

One goal of the present IRIS experiments was to compare the surface interactions of multiple radicals in FC depositing plasmas under the same conditions to develop a deeper understanding of how the interfacial reactions of different radicals affect the FC film properties. Thus, we have measured CH, C_3, CHF, and CF_2 scattering coefficients and surface reactivities during the deposition of FC films with a range of compositions using CH_2F_2/C_3F_8 plasmas. We have also measured the relative gas-phase densities for both ground- and excited-state species as a function of the CH_2F_2/C_3F_8 ratio in the feed gas using LIF and optical emission spectroscopy (OES), respectively. Correlations are made between the surface reactivity measurements of these radicals and the FC film surface properties as measured by XPS.

II. EXPERIMENTAL DETAILS

The IRIS apparatus has been described in detail previously (6, 29). Briefly, IRIS uses molecular beams and LIF to measure the steady-state surface reactivity of gas-phase species during film deposition, as well as the relative gas-phase density of plasma species as a function of different plasma parameters [applied radio-frequency (RF) power (*P*), pressure, and gas composition], and substrate bias. A nickel-plated copper coil is used to couple 13.56 MHz rf power to a cylindrical, glass tubular reactor to create a plasma. Expansion of the plasma through a differentially pumped high-vacuum system generates an effusive molecular beam, which contains virtually all of the species present in the plasma. For reactivity measurements, the molecular beam is collimated by two slits mounted on a liquid-nitrogen-cooled shield, which can be maintained at −160 °C during data collection. This serves to minimize spurious scattering off the differential wall. A tunable excimer-pumped (XeCl) dye laser beam intersects the molecular beam at a 45° angle downstream from the plasma source and excites the selected molecule. Spatially resolved LIF signals are collected by a gated, intensified charge-coupled device (ICCD) located perpendicular to both the molecular beam and the laser beam, directly above the interaction region. In general, the ICCD camera had a 2.0−3.0 μs gate width and a 1.70 μs gate delay, which were largely determined by the fluorescence lifetime of the specific molecule under study.

For rotational excitation spectra, tunable laser light is produced from an excimer-pumped dye laser. The total fluorescence produced by a particular radical transition is collected and plotted as a function of the laser wavelength. For relative density and reactivity measurements, the LIF intensity produced by a particular transition is collected as a function of the plasma parameters, such as the feed gas composition or *P*. Steady-state surface reactivity measurements are performed by setting the laser to a particular absorption frequency for the molecule of interest. The spatially resolved LIF intensity was collected; a substrate was then rotated directly into the path of the molecular beam, situated at a known distance from the laser beam (3.0−3.6 mm), and LIF signals were again collected. Differences between the spatial distributions with the surface in and out of the path of the molecular beam were used to measure radical−surface reactivity. Background images, acquired with the laser tuned to an off-resonance wavelength, were subtracted from the corresponding on-resonance image. For CHF reactivity measurements, background images were collected with the laser off because the off-resonance images contained significant spurious light signals. A one-dimensional cross section of the image was made by averaging 20 columns of pixels (7.7 mm) containing the LIF signal and plotting the signal intensity as a function of the distance along the laser beam path. To ensure that steady-state conditions had been reached, the substrates were exposed to the plasma molecular beam for 10−30 min before beginning IRIS measurements, allowing several nanometers of film to be deposited on the surface.

A numerical simulation based on the experimental geometry of the IRIS apparatus is used to quantify the molecular scatter from the LIF signals acquired (30). The simulation calculates the spatial distribution of the radical number density in the molecular beam at the interaction region as well as the radical number density along the laser axis for molecules scattering from the substrate surface, assuming an adsorption−desorption scattering mechanism. The calculated curve for this type of scatter assumes that all incident radicals leave the surface with a cosine distribution about the surface normal. To determine the surface reactivity of a specific molecule, the fraction of radicals scattering from the surface, *S*, is adjusted to best fit the experimental data. The steady-state surface reactivity, *R*, is defined as $1 - S$. Clearly, when $S > 1$, surface generation of the radical is occurring (6, 31, 32). Similarly, when $S < 1$, the molecules are lost at the surface during deposition, presumably via incorporation into the growing film. Note, however, that IRIS measurements do not track a single molecule, so reaction of the species under study to form a volatile species that desorbs from the surface cannot be excluded. To further establish the contributions of other plasma species on the observed reactivities, ion effects on scattering values were studied by applying +200 V bias on the substrate to repel positively charged species (6, 31, 33).

ARTICLE

Table 1. IRIS Conditions for Radical Reactivity Measurements

radical	transition	radiative lifetime	wavelength (nm) on-resonance	wavelength (nm) off-resonance	laser dye	slit sizes (nm) first	slit sizes (nm) second	liquid nitrogen cooling (°C)	ICCD camera gate width	ICCD camera gate delay
CH	$A^2\Delta \rightarrow X^2\Pi$	537 ns[53]	430.402	430.200	Coumarin 440	1.60	1.70		2.0 μs	1.68μs
C_3	$^1\Pi_u \rightarrow {}^1\Sigma_g^+$	200 ns(54)	404.993	405.140	Exalite 404	1.75	1.70	−160	2.5 μs	1.77μs
CHF	$\tilde{A}^1A''(000) \rightarrow X^1A'(000)$	2.45 μs[39]	579.120	Laser off	Rhodamine 590	1.60	1.70		3.0 μs	1.78μs
CF_2	$A^1B_1 \rightarrow X^1A_1$	61 ns(44)	234.323	235.000	Coumarin 47	1.0−1.1	1.2−1.4	−160	100 ns	1.65μs

The surface reactivities of CH, C_3, CHF, and CF_2 radicals were measured at the surface of a growing FC film in CH_2F_2/C_3F_8 plasmas with different gas ratios. Relevant IRIS conditions for the reactivity measurements of these species are listed in Table 1, along with their radiative lifetimes (26−29). The total fluorescence was collected over a time period that was longer than the entire radiative lifetime of each species. Tunable laser light for the excitation of a particular radical was produced using different laser dyes (Table 1). The plasma molecular beam was collimated by two slits, 1.0−1.75 and 1.2−1.7 mm wide, respectively, with the second slit located 12 mm downstream from the first slit. For C_3 and CF_2 reactivity measurements, the two slits were cooled to minimize the effects from signals of molecules scattering off of the slits (30, 34−36). The CH and CHF species do not have large scattering signals; thus, the slits were not cooled so as to maximize the signal intensity for these two molecules.

The FC films deposited on the substrate in the IRIS apparatus at different gas compositions were analyzed by XPS using a Physical Electronics PE5800 ESCA/Auger electron spectroscopy system. Survey scans (0−1000 eV) acquired with an analyzer pass energy of 93.9 eV were used to determine the elemental composition. A photoelectron take-off angle of 45° was used for all spectra. High-resolution C 1s spectra were decomposed to analyze the C-bonding environment in the films. Specifically, CF_3 (293.9−294.2 eV) and CF_2 (291.8−291.4 eV) groups function as chain-termination and chain-elongation groups, respectively, whereas $-\underline{C}F-CF$ (289.4−288.7 eV), $\underline{C}-C_xF_y$ (287.3−286.7 eV), and $\underline{C}-H$ (285.7 eV) species contribute to cross-linking and branching in the film (16, 30). Note that the spectra were corrected for surface charging by setting the hydrocarbon component to 285.7 eV.

OES data were collected in an independent inductively coupled plasma reactor (37, 38) similar to the source for the IRIS apparatus. The reactor was fitted with a replaceable fused quartz window at the downstream end, allowing for the coaxial collection of plasma emission for maximum signal intensities. Plasma emission was imaged onto the 10 μm entrance slit of an Avantes multichannel spectrometer fitted with four optical fibers fused into one cable. The spectrometer houses four fiber gratings, yielding a 0.1 nm resolution, four 3648 pixel charged-coupled device array detectors, and a wavelength detection range from 187 to 1016 nm. Emission signal integration times were set to 10 ms. Actinometry was used to provide comparative, quantitative data on the species of interest in our IRIS experiments. Thus, small amounts (3−5%) of argon (actinometric signal for Ar* at 750.4 nm) were added to the CH_2F_2/C_3F_8 plasmas (38). In its simplest form, the ratio of the emission intensity from the excited-state species of interest (I_x) to that of an actinometer (I_{act}) is taken as the relative number density for the species of interest (12). Here, we used signals at the following wavelengths for the respective molecules: 340.94 nm (CF_2), 405.08 nm (C_3), 431.34 nm (CH), and 578.5 nm (CHF) (12, 39−41).

III. RESULTS

The spectral selectivity of LIF allows identification and independent study of a specific radical in a molecular beam containing many different species. In principle, the tunable XeCl dye laser beam (200−800 nm) can selectively excite various radicals during film deposition for IRIS measurements. LIF excitation spectra for CF_2, CH, and C_3 recorded in our IRIS instrument have been described previously (6, 42, 43). With all three molecules, a comparison to literature spectra verified that the fluorescing species was identified correctly. Similar spectra were acquired here prior to performing reactivity measurements (not shown). Because CHF is the only molecule studied here that has not previously been characterized in our IRIS apparatus, we collected extensive fluorescence excitation spectra for this molecule, an example of which is shown in Figure 1. A comparison to literature spectra verifies that the fluorescing species is indeed CHF (44). All CHF reactivity data presented here were taken with the laser tuned to the band at 579.13 nm, corresponding to the wavelength of the $^PQ_1$ band origin of the CHF $\tilde{A}^1\tilde{A}''(000) \leftarrow \tilde{X}^1A'(000)$ transition.

One key to understanding the FC deposition processes is determining formation mechanisms for potential deposition precursors. Here, we determined the relative amounts of CH, C_3, CF_2, and CHF radicals as a function of the

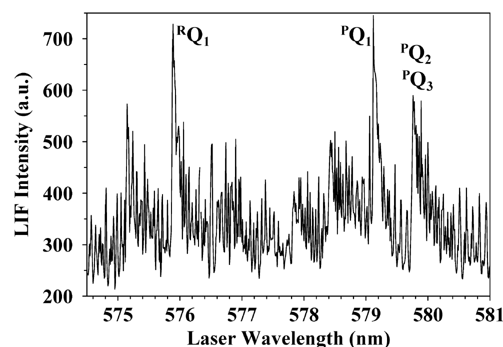

FIGURE 1. Laser excitation spectrum of the CHF $\tilde{A}^1A''(000) \leftarrow \tilde{X}^1A'(000)$ transition, with positions of the Q branch band heads marked. For this spectrum, CHF was formed from a CH_2F_2 plasma at P = 50 W and a pressure of 100 mTorr. The spectrum was acquired by stepping the laser from 574.5 to 581 nm in 0.01 nm increments.

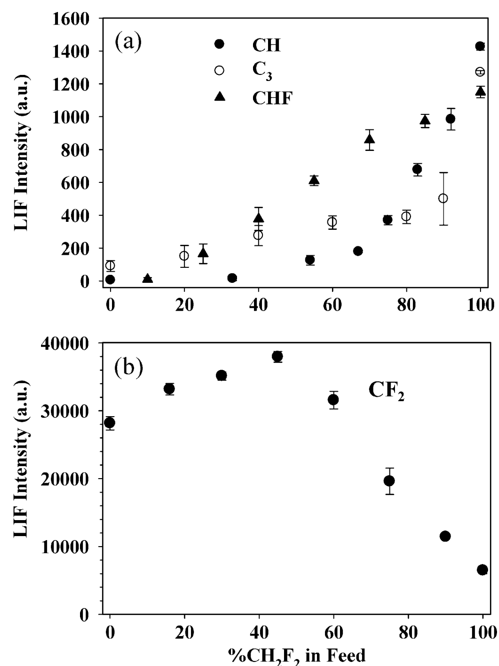

FIGURE 2. LIF intensities as a function of the CH_2F_2 fraction in the feed gas for (a) CH in CH_2F_2/C_3F_8 plasmas at a total pressure of 120 mTorr and $P = 120$ W along with C_3 and CHF in CH_2F_2/C_3F_8 plasmas at a total pressure of 100 mTorr and $P = 100$ W and (b) CF_2 in CH_2F_2/C_3F_8 plasmas at a total pressure of 100 mTorr and $P = 100$ W.

deposition parameters, most notably gas ratios. Figure 2 contains CH, C_3, CF_2, and CHF LIF intensities as a function of the CH_2F_2 fraction in CH_2F_2/C_3F_8 plasmas. Data for the CH radical were acquired at slightly higher *P* and pressure to maximize the signal intensity. As expected, the signal intensities for all four molecules show a clear dependence on the CH_2F_2 fraction. Specifically, the densities of CH, C_3, and CHF in the mixed-gas plasmas increase when the CH_2F_2 fraction increases from 0 to 100% (Figure 2a). At low CH_2F_2 fractions, the amount of CH is virtually zero, rising sharply as the % CH_2F_2 increases above ~50%. The C_3 density increases only slightly with the CH_2F_2 fraction, whereas that for CHF increases substantially from % CH_2F_2 = 10 to % CH_2F_2 = 90. This suggests that the CH and CHF molecules are formed solely from the CH_2F_2 precursor, whereas C_3 is likely formed by multiple reactions in the gas phase of the plasma but is clearly directly related to the CH_2F_2 precursor. The CF_2 LIF intensities are plotted as a function of % CH_2F_2 in Figure 2b. Note that, although not absolute, the raw intensities for CF_2 are more than an order of magnitude larger than any of the other three species, suggesting this is the predominant species in all of these plasmas. These results are consistent with previous mass spectrometry results from our laboratory, which show that CF_2 is present in C_3F_8 plasmas (6, 28). Moreover, the CF_2 LIF intensity increases somewhat with an increased CH_2F_2 fraction in the feed (up to ~40%) and then decreases at CH_2F_2 fractions above 45%. Thus, it is the decomposition of the C_3F_8 precursor that contributes most significantly to CF_2 production in the plasma. Small additions of CH_2F_2 do, however, contribute to an increase in the CF_2 density, suggesting that some CF_2 arises from this precursor.

The LIF density data provide information on the ground-state species in the plasma. It is also useful to examine the emission intensities of the same species (CH, C_3, CF_2, and CHF) to show the variation in excited-state species production as the feed gas composition is varied. In mixtures consisting primarily of C_3F_8 (Figure 3a), a prominent CF_2 band exists at 250−350 nm. As the C_3F_8 concentration in the feed is decreased (Figure 3b), the CF_2 band effectively disappears, indicating significant changes in excited-state species production within the plasma. Actinometric OES data provide a quantitative illustration of molecule production as the feed gas ratio is varied (Figure 3c,d). The formation of two species, C_3* and CH*, is not highly dependent on % CH_2F_2 in the feed (Figure 3c), suggesting that these species do not arise preferentially from either precursor gas. Note that there is a somewhat more pronounced dependence on the feed gas composition for emission from F atoms in the plasma, with more signals arising in plasmas with higher CH_2F_2 content. Although CHF* has a slight dependence on the feed gas ratio (Figure 3c), increasing slightly at higher CH_2F_2 concentrations, the overall intensity is much smaller than that of either C_3* or CH*. The lack of a strong dependence of CHF* and CH* production observed in the OES contrasts sharply with the LIF data for ground-state species (Figure 2a). Figure 3d shows the actinometric OES data for CF_2 and H_α in the FC plasmas. For CF_2, the data demonstrate a gas ratio dependence nearly identical with that observed in the LIF data (Figure 2b), supporting the hypothesis that C_3F_8 is the precursor responsible for CF_2 production. Interestingly, the data for the H_α emission show the opposite trend with a nearly monotonic increase in the signal as the fraction of C_3F_8 in the feed decreases.

The surface reactivity in IRIS experiments is measured by a comparison of the ICCD images obtained with the substrate in and out of the path of the plasma molecular beam. Figure 4 shows a series of ICCD images for CH in an 80 W, 100/20 mTorr CH_2F_2/C_3F_8 plasma. The LIF signal from CH in the molecular beam is shown in Figure 4a. Figure 4b contains the LIF signal acquired with a silicon substrate rotated into the path of the molecular beam, imaging both the incident and scattered CH radicals. Figure 4c is the difference between parts b and a of Figure 4, revealing only a slight signal arising from CH desorbing from the surface. Figure 5 shows the same series of IRIS images for CHF from a 100 W, 30/70 mTorr CH_2F_2/C_3F_8 plasma molecular beam interacting with a silicon substrate. The difference between the images shown in parts a and b of Figure 5 provides a spatially resolved image of CHF radicals scattered from the FC growing surface (Figure 5c). In contrast to the image shown in Figure 4c, there is clearly a considerable amount of CHF emanating from the surface.

To quantify the amount of scatter for a set of reactivity data, a cross section of 20 columns of pixels were averaged and plotted as a function of the distance along the laser axis. Cross-sectional data for all four molecules are shown in Figure 6. Figure 6a contains the cross sections of the LIF images of CH shown in Figure 4a,c. Also shown in Figure

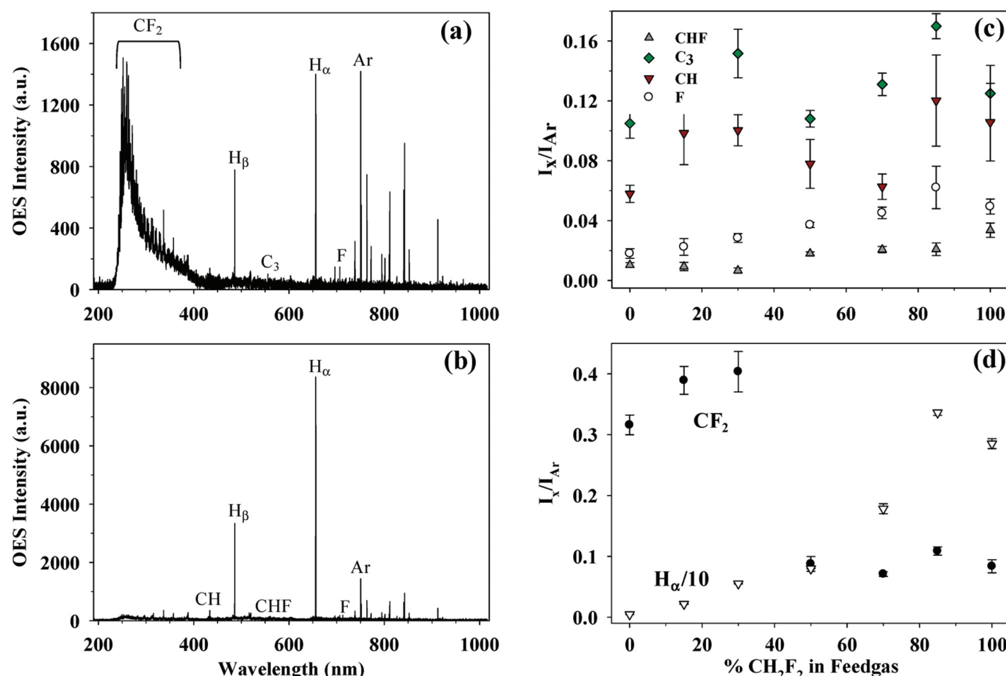

FIGURE 3. OES spectra of mixtures of FC plasmas ($P = 100$ W, total pressure of 100 mTorr) with mixtures of (a) 30/70 mTorr CH_2F_2/C_3F_8 and (b) 85/15 mTorr CH_2F_2/C_3F_8. Actinometric OES data as a function of the CH_2F_2 fraction in the feed gas are shown for (c) CH, CHF, C_3, and F atoms and (d) CF_2 and H_α atoms. Note that the H_α data have been decreased by a factor of 10 in this plot. Error bars represent 1 standard deviation from the mean of three trials.

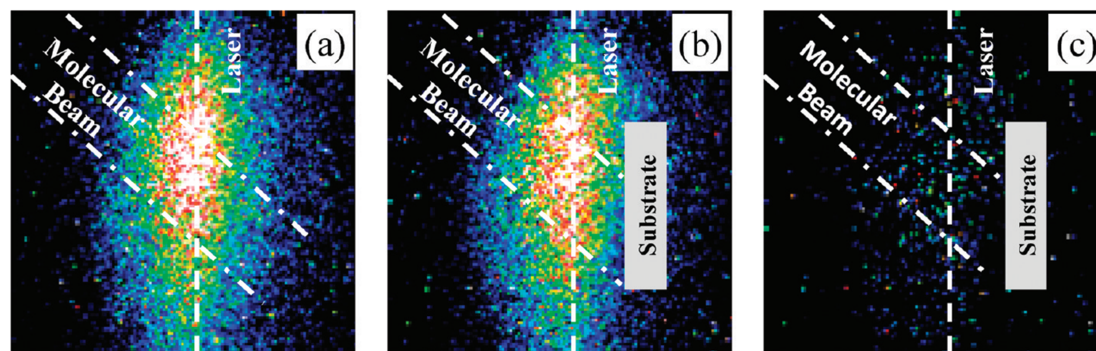

FIGURE 4. ICCD images of CH LIF signals in (a) a 80 W, 100/20 mTorr CH_2F_2/C_3F_8 plasma molecular beam and (b) with a silicon substrate rotated into the path of the molecular beam. The image shown in part c is the difference between the images in parts a and b and corresponds to CH radicals scattered from the surface. Dashed lines indicate the locations of the molecular beam and the laser beam.

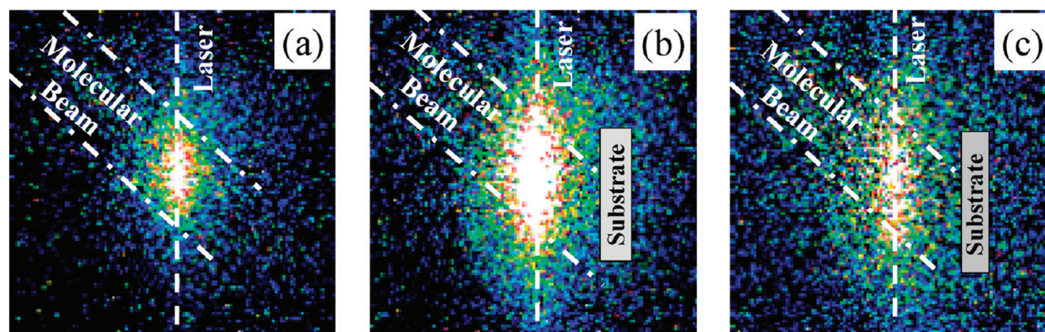

FIGURE 5. ICCD images of CHF LIF signals in (a) a 100 W, 30/70 mTorr CH_2F_2/C_3F_8 (total pressure 100 mTorr) plasma molecular beam and (b) with a silicon substrate rotated into the path of the molecular beam. The image shown in part c is the difference between the images in parts a and b and corresponds to CHF radicals scattered from the surface. Dashed lines indicate the locations of the molecular beam and the laser beam.

6a are simulated curves for molecules in the incident beam and for scattered CH, assuming an adsorption−desorption mechanism, with $S = 0.05 \pm 0.05$. This value is consistent with previous IRIS measurements for CH formed from CH_4 plasmas (43). Parts b−d of Figure 6 provide representative sets of experimental cross sections and simulated curves for C_3 radicals from a 80 W, 13/87 mTorr CH_2F_2/C_3F_8 plasma, CF_2 from a 100 W, 40/60 mTorr CH_2F_2/C_3F_8 plasma, and

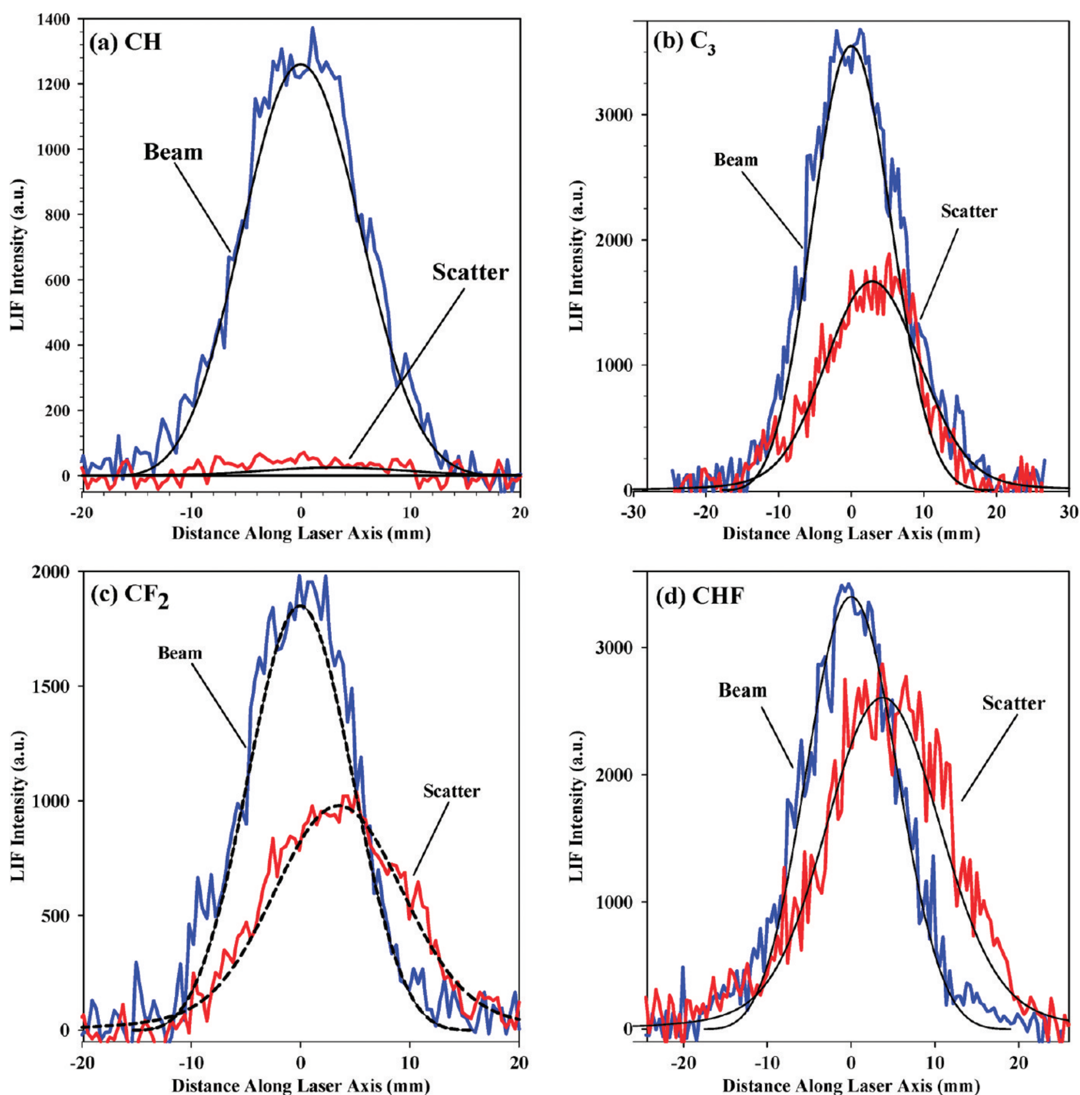

FIGURE 6. Representative sets of experimental data (molecules in incident molecular beams and scattered from a 300 K silicon substrate) and simulated curves for IRIS data acquired for (a) CH produced in a 80 W, 100/20 mTorr CH_2F_2/C_3F_8 plasma, (b) C_3 produced in a 80 W, 13/87 mTorr CH_2F_2/C_3F_8 plasma, (c) CF_2 produced in a 100 W, 40/60 CH_2F_2/C_3F_8 plasma, and (d) CHF produced in a 100 W, 30/70 mTorr CH_2F_2/C_3F_8 plasma. In all systems, the plasma molecular beams were impinging on +200 V biased room-temperature silicon substrates and a-F:C films were being deposited on the substrates.

CHF radicals from a 100 W, 30/70 mTorr CH_2F_2/C_3F_8 plasma, respectively. The Figure 6 data demonstrate that the different radicals studied have very different scatter coefficients during FC film growth. In particular, it is clear that CH is much more reactive than the other three molecules. The averages of several data sets for the conditions provided in Figure 6 yield $S(CH) = 0.05 \pm 0.07$, $S(C_3) = 0.68 \pm 0.09$, $S(CF_2) = 0.84 \pm 0.11$, and $S(CHF) = 1.40 \pm 0.05$. These correspond to surface reactivities or surface loss coefficients of $R(CH) = 0.95 \pm 0.07$, $R(C_3) = 0.32 \pm 0.09$, and $R(CF_2) = 0.16 \pm 0.11$. Note that the S(CHF) value is greater than 1, indicating that a net surface generation of CHF occurs during film growth under these conditions. In contrast, the extremely high R(CH) values clearly suggest that CH radicals are active during film growth. The intermediate values found for C_3 and CF_2 are indicative of moderate surface reactivity.

The effects of the CH_2F_2 fraction, substrate bias, and P on the surface reactivities of CH, C_3, CF_2, and CHF radicals were measured, and the resulting S values are listed in Table 2. Note that P-dependence measurements were only performed for the CH molecule. The scattering coefficients of CH do not show any dependence on the feed gas composition, substrate bias, or P. Indeed, S(CH) values are all less than about 0.05 ± 0.07, indicating that virtually all of CH is lost at the surface during FC film deposition. Again, this is consistent with our previous measurements for CH in other plasma systems (43) and also correlates with the results for the isoelectronic SiH molecule in silane systems (45). The $S(C_3)$ values (0.62−0.90) also do not show a clear dependence on the gas composition or substrate bias, although they do vary somewhat depending on conditions. Scatter coefficients for C_3 measured with a +200 V bias are slightly elevated from those acquired with a grounded substrate. These values indicate the moderate surface reactivity of C_3 radicals during FC film deposition.

In contrast, the scattering coefficients for CF_2 appear to have some dependence on substrate bias. Specifically, applying a +200 V bias on the substrate leads to a significant

ARTICLE

Table 2. Surface Scattering Coefficient (S) Values for Species in CH_2F_2/C_3F_8 Plasmas

species	CH_2F_2/C_3F_8 gas ratio (mTorr)	bias (V)	P (W)	S^a
CH	120/0	0	80	0.00 (0.04)
	120/0	200	80	0.03 (0.04)
	100/20	0	80	0.02 (0.05)
	100/20	200	80	0.03 (0.05)
	80/40	0	80	0.04 (0.05)
	80/40	200	80	0.02 (0.06)
	120/0	0	120	0.00 (0.06)
	120/0	200	120	0.05 (0.05)
	100/20	0	120	0.01 (0.06)
	100/20	200	120	0.05 (0.05)
	80/40	0	120	0.01 (0.03)
	80/40	200	120	0.03 (0.05)
$C_3{}^b$	100/0	0	80	0.86 (0.07)
	100/0	200		0.90 (0.06)
	87/13	0		0.62 (0.11)
	87/13	200		0.68 (0.09)
	70/30	0		0.72 (0.07)
	70/30	200		0.88 (0.11)
	50/50	0		0.62 (0.11)
	50/50	200		0.67 (0.08)
CF_2	0/100	200	100	0.70 (0.05)
	0/100	0		1.31 (0.06)
	40/60	200		0.84 (0.11)
	40/60	0		0.87 (0.10)
CHF	85/15	0	100	1.65 (0.06)
	70/30	0		1.40 (0.05)
	65/35	0		1.32 (0.07)
	50/50	0		1.40 (0.15)
	30/70	0		1.25 (0.15)
	15/85	0		1.00 (0.15)
	85/15	200		1.70 (0.05)
	70/30	200		1.40 (0.05)
	65/35	200		1.50 (0.10)
	50/50	200		1.40 (0.12)
	30/70	200		1.35 (0.12)
	15/85	200		1.10 (0.17)

[a] Errors for S values (given in parentheses) are the standard deviation of the mean of a minimum of three values. [b] These values have been reported previously (42).

reduction in the S values when a 100% C_3F_8 plasma is used. The $S(CF_2) > 1$ value measured without substrate bias indicates net surface production of CF_2 during FC film deposition, which is consistent with the results reported previously (34). Mass spectra of positive ions in the C_3F_8 plasma molecular beams indicate that the major ionic constituents are CF^+, $CF_2{}^+$, and $CF_3{}^+$ (33). All ions have broad, complex energy distributions with mean ion energies ranging from 28 to 92 eV, depending on P and the gas pressure. These energetic ions have sufficient energy to break chemical bonds in FC films, one possible mechanism for the observed surface production of CF_2. The +200 V substrate bias effectively repels positive ions from reaching the substrate, such that "ion-free" conditions are created. The $S(CF_2) < 1$ values measured with CH_2F_2/C_3F_8 mixtures

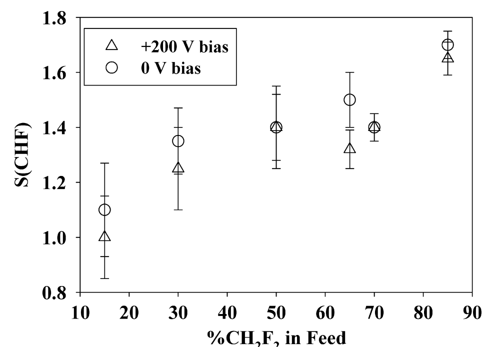

FIGURE 7. Surface scatter coefficients for CHF, S(CHF), as a function of the CH_2F_2 fraction in the feed gas. Data shown were acquired using either a 300 K grounded substrate (open circles) or a 300 K, +200 V substrate (open triangles).

indicate that CF_2 radicals are reactive during FC film deposition in this system.

S(CHF) values show a clear dependence on the gas composition, increasing from 1.10 ± 0.17 at % $CH_2F_2 = 15$ to 1.70 ± 0.05 at % $CH_2F_2 = 85$, for substrates with no bias (Figure 7). Also shown in Figure 7 are the S(CHF) values for measurements made with a +200 V substrate bias. Interestingly, these values are not statistically different from those measured on the unbiased substrates. Note $S(CHF) > 1$ under nearly all conditions, indicating that net surface production of CHF occurs during FC film deposition. Interestingly, this observation tracks with the OES data in Figure 3, which clearly shows that the gas-phase concentration of F and H atoms also increases with % CH_2F_2 in the feed.

XPS analysis of the FC films deposited in the IRIS apparatus using CH_2F_2/C_3F_8 plasmas provides elemental and structural data. High-resolution C 1s spectra of FC films deposited at four different CH_2F_2/C_3F_8 ratios are shown in Figure 8. Although all of these films can be considered to be amorphous fluorinated, hydrogenated carbon films (a-C:F,H), some distinctions can be made between the materials. Parts a and b of Figure 8 contain spectra of FC films deposited with % CH_2F_2 = 0 and 12, respectively. These films clearly contain a variety of CF_x moieties, including $\underline{C}F_3$, $\underline{C}F_2$, $\underline{C}F$, and $\underline{C}-CH_xF_y$. Increasing the % CH_2F_2 to 88 and 100 (parts c and d of Figure 8, respectively) yields films with a marked increase in the amount of $\underline{C}-CH_xF_y$ and $\underline{C}H$ functionalities. The spectrum of the film deposited from a 100% CH_2F_2 plasma (Figure 8d) is dominated by CH and $C-CH_xF_y$ moieties, with little contribution from CF_x groups. In FC films, CF_3 and CF_2 groups function as chain-termination and chain-elongation groups, respectively (9, 10). In contrast, $-\underline{C}F-CF$, $-\underline{C}F-C$, $\underline{C}-C_xF_y$, and $\underline{C}-H$ are considered species that contribute to cross-linking and branching in the film (9, 10). Thus, increasing the CH_2F_2 content of the plasma contributes to the deposition of FC films with more cross-linked structure.

IV. DISCUSSION

Film growth via PECVD is a complex process involving a wide range of molecule−surface interaction and interfacial processes that are often difficult to fully characterize. These

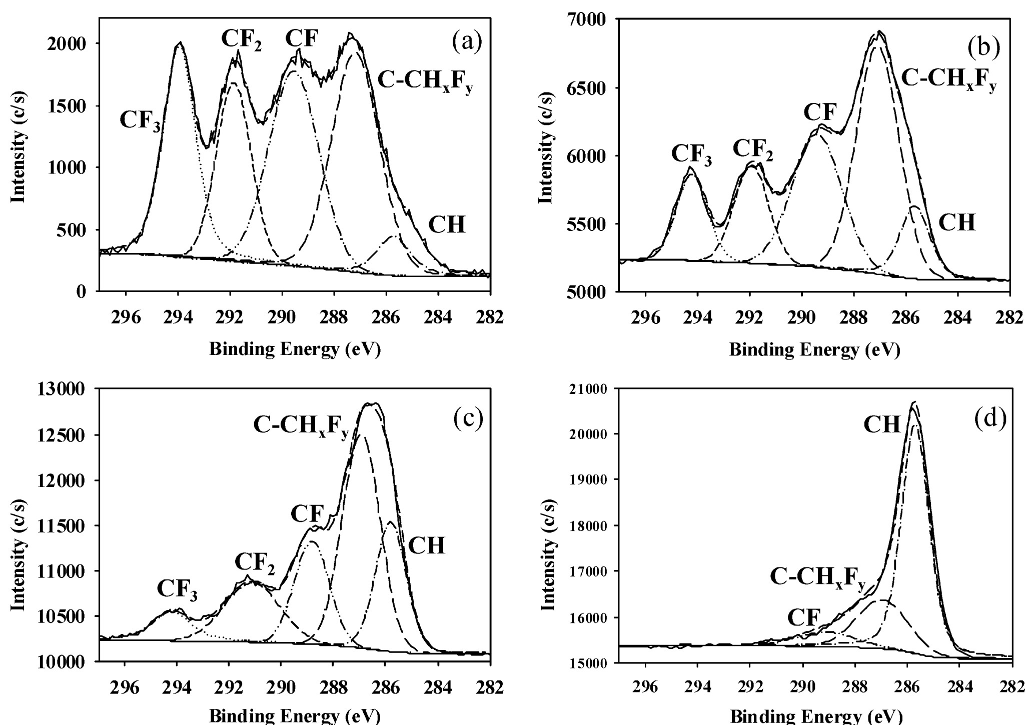

FIGURE 8. High-resolution C 1s spectra of FC films deposited at different CH_2F_2/C_3F_8 ratios ($P = 100$ W): (a) 0/100 mTorr; (b) 12/88 mTorr; (c) 88/12 mTorr; (d) 100/0 mTorr.

processes include radical−surface reactions and energetic ion bombardment that serve to create radical sites in the growing film surface. Subsequent molecule−surface interactions can result in the recombination or termination of those radical sites. In FC systems, unraveling the interface chemistry becomes more problematic because substrate etching and film deposition are competing processes that occur simultaneously (15). Understanding molecule−surface interactions for multiple species present in these systems is one step toward developing a deeper knowledge of the overall mechanisms controlling plasma−surface interactions.

Our previous IRIS measurements in FC systems have focused on CF_2 and have been performed using plasmas formed from a single precursor such as CHF_3, HFPO, C_3F_8, or C_4F_8 (13, 26, 28, 46). In nearly all systems, CF_2 is generated at the surface during plasma processing. Moreover, creating "ion-free" conditions using a variety of different techniques, including placing a grounded mesh screen in the path of the molecular beam as well as +200 V biasing of the substrate, suggests that the observed CF_2 surface generation is the result of ion bombardment of the depositing FC film. Using a hot-filament CVD source that does not produce ions that can react or physically sputter the deposited film, we observed a near-unity scattering coefficient for CF_2 but no surface production (26). Here, our IRIS measurements of CF_2 in the mixed FC plasmas also indicate a very low surface reactivity of CF_2 or surface production in the case of the 100% C_3F_8 plasma. One possible explanation for this low reactivity of CF_2 is that CF_2 may only contribute to film deposition when adsorbing to radical sites that have been created on the film surface during ion bombardment. It should also be noted that $R(CF_2)$ values of ∼0.2 have been observed previously in our laboratories when a-C:F,H films are produced from 50/50 C_2F_6/H_2 plasmas (47), consistent with the values determined here using a 40/60 CH_2F_2/C_3F_8 plasma (Table 2).

Our IRIS measurements indicate that $S(CHF) \geq 1$ under all conditions studied here, suggesting that CHF can be generated during radical−surface reactions, similar to the CF_2 molecule. CHF is likely formed in the gas phase of the plasma through an electron impact reaction such as process (1), which also leads to formation of a stable HF molecule.

$$CH_2F_2 + e^- \rightarrow CHF + HF + e^- \quad (1)$$

The strong dependence of the CHF LIF signal on % CH_2F_2 in the feed clearly indicates that CHF is formed via the direct dissociation of CH_2F_2 and is not likely the result of secondary gas-phase recombination reactions between previously formed fragment species. Similar to results for CF_2, CHF may also contribute to film growth when reacting at radical sites created at the surface of the growing film. Previous IRIS measurements in our laboratory on a wide range of plasma species indicate that a radical's surface reactivity may be related to the radical's electronic configuration and stability (27, 48). For example, both CHF and CF_2 have singlet electronic configurations and both species exhibit low surface reactivities. Examination of the C 1s XPS data for films deposited in our mixed CH_2F_2/C_3F_8 plasmas yields some additional insight into possible mechanisms for the surface production of CHF. Specifically, for films deposited in these systems, in addition to CF_x ($x = 1-3$) groups, comparable concentrations of CH_x ($x = 1-3$) groups are also found.

Highly reactive gas-phase F or H atoms can react with the bonded $-CH_xF_y$ ($x = 0, 1$; $y = 0, 1$) at the depositing film surface, as shown in processes (2)−(5).

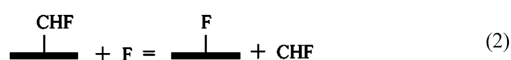

(2)

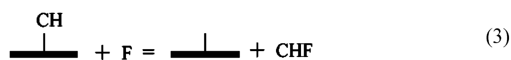

(3)

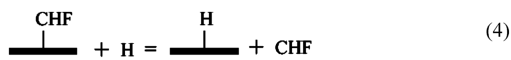

(4)

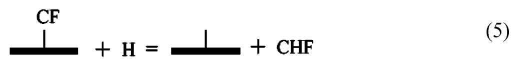

(5)

These reactions are likely large contributors to the observed surface generation of CHF. Interestingly, our work with CF_2 molecules has indicated that conditions leading to highly cross-linked films result in higher $S(CF_2)$ values (28). This general trend appears to hold for S(CHF) molecules as well. Additional studies are currently underway to examine the P dependence of both CHF and CF_2 in these systems because previous studies in our group have shown that significantly more scatter is observed for singlet molecules at higher applied rf powers if the molecule is formed via surface generation (6, 28, 31, 32).

The third molecule studied here with a singlet electronic configuration is C_3. Formation of C_3 in the gas phase of the plasma must proceed via a series of reactions. One possible scenario involves the electron impact dissociation to form gas-phase C atoms, process (6). Dimerization of carbon has been confirmed experimentally to occur via reaction (7) (49).

(6)

(7)

Subsequently, C_3 is primarily produced in the gas phase by three-body reactions between C atoms and C_2, process (8) (50).

(8)

Our LIF density data demonstrate that the C_3 content in the plasma rapidly increases with an increase in the CH_2F_2 fraction (Figure 2a). Although the dependence appears to be less dramatic, a similar trend is observed for C_3* in the OES data (Figure 3c). Similar to the other singlet molecule studies here, C_3 exhibits a fairly low surface reactivity ($R \sim 0.1$) in the 100% CH_2F_2 plasma. At lower concentrations of CH_2F_2 in the feed, C_3 reactivity does increase, with the highest R value measured at ∼0.38. Interestingly, $R(C_3)$ does not exhibit clear trends with any of the parameters examined thus far (i.e., gas ratio, substrate bias, etc.) (42). The arguably moderate reactivities found for the C_3 molecule do, however, suggest that it is an active species in the deposition of a-C:F,H films in these systems, consistent with the results of van de Sanden and co-workers (51). Again, additional P-dependence studies would lend further insight into the surface interactions of this species.

The fourth molecule studied here, CH, has a doublet configuration, unlike the other three molecules. In the plasma, CH radicals are likely produced during energetic collisions of electrons with CH_2F_2 molecules, as suggested by the strong dependence of the CH density on the CH_2F_2 concentration (Figure 2a). The surface reactivity of CH radicals has been previously measured during the deposition of hydrogenated diamondlike carbon films using CH_4 rf plasmas (43). Consistent with the present results (Table 2), the measured surface reactivity of CH in methane-based systems was near unity and showed no dependence on the applied rf power, feed gas composition, or substrate bias. Notably, we have recently reported similar results for CN radicals, which also have a doublet electronic configuration in amorphous carbon nitride (a-C:N) film deposition using CH_3CN plasmas (52). Specifically, CN reacts with high probability (S(CN) ∼0.8) at the growing a-C:N film surface and is not dependent on any experimental parameters. In the CH_3CN system, we believe CN radicals are the major source of the nitrogen content of the films. In the FC systems studied here, CH radicals are likely contributing to the growing a-C:F,H film via reactions with radical sites on the surface, insertion into C−H or C−F bonds on the surface, or surface-induced dissociation. Alternatively, another possible surface loss mechanism is CH abstraction of a surface fluorine (or hydrogen) and desorption of CHF (or CH_2), process (9).

(9)

Process (9) would also contribute to the observed surface generation of CHF during film formation. Overall, it appears that CH and C_3 contribute to the formation of a-C:F,H films in these systems, whereas CHF and CF_2 are not dominant film precursors. As a final note, this work has focused on only four plasma species in these systems. Clearly, other plasma species such as CF and CF_3 are also possible film precursors in these systems. Moreover, the observed surface generation of CF_2 and CHF could arise from the surface interactions of plasma species such as CF_3 and CF or ionic species such as CF_3^+, CF_2^+, or CF^+. Dissociation, surface atom abstraction, and neutralization of ionic species at the surface are all possible mechanisms that could account for all or some of the observed surface generation in these systems. IRIS measurements are currently underway to explore at least some of these species, most notably CF and the effect of ionic species on the measured surface interactions.

V. SUMMARY

We have investigated the gas-phase density of various carbon-containing species, specifically CH, C_3, CHF, and CF_2, using OES and LIF. These data demonstrate that both the ground and excited states of CF_2 and CHF have a strong dependence on the feed gas composition. In contrast, the formation of CH* and C_3* in the plasma does not exhibit a

strong dependence on the feed gas concentration, whereas the formation of the ground-state CH and C_3 species does, with much higher C_3 signals arising from high CH_2F_2 content plasmas. We have also measured the surface interactions of these species during PECVD of FC films using CH_2F_2/C_3F_8 plasmas with different gas ratios. These IRIS data offer an opportunity to explore the effects of various radicals on the FC film deposition. A surface reactivity of nearly unity has been observed for CH, a radical with a doublet electronic configuration, whereas the plasma species with singlet electronic configurations, CF_2, CHF, and C_3, exhibit very low surface reactivity or surface generation during a-C:F,H formation. Additional IRIS experiments currently underway in our laboratory will allow for further exploration of the hypothesis that a molecule's surface interactions can be predicted by its electronic configuration.

Acknowledgment. Financial support for this work came from the National Science Foundation (Grant NSF-0613653).

REFERENCES AND NOTES

(1) Rothman, L. B. *J. Electrochem. Soc.* **1980**, *127*, 2216.
(2) Sun, S. P.; Muraka, S. P.; Lee, C. J. *J. Vac. Sci. Technol.* **1988**, *6*, 1963.
(3) Tokahashi, K.; Mitamura, T.; Ono, K.; Setsuhara, Y.; Itoh, A.; Tachibana, K. *Appl. Phys. Lett.* **2003**, *82*, 2476.
(4) Mackie, N. M.; Dalleska, N. F.; Castner, D. G.; Fisher, E. R. *Chem. Mater.* **1997**, *9*, 349.
(5) Butoi, C. I.; Mackie, N. M.; Williams, K. L.; Capps, N. E.; Fisher, E. R. *J. Vac. Sci. Technol. A* **2000**, *18*, 2685.
(6) Martin, I. T.; Fisher, E. R. *J. Vac. Sci. Technol. A* **2004**, *22*, 2168.
(7) Takahashi, K.; Tachibana, K. *J. Appl. Phys.* **2001**, *89*, 893.
(8) Labelle, C. B.; Limb, S. J.; Gleason, K. K. *J. Appl. Phys.* **1997**, *82*, 1784.
(9) Butoi, C. I.; Mackie, N. M.; Barnd, J. L.; Fisher, E. R.; Gamble, L. J.; Castner, D. G. *Chem. Mater.* **1999**, *11*, 862.
(10) Butoi, C. I.; Mackie, N. M.; Gamble, L. J.; Castner, D. G.; Barnd, J.; Miller, A. M.; Fisher, E. R. *Chem. Mater.* **2000**, *12*, 2014.
(11) Labelle, C. B.; Gleason, K. K. *J. Appl. Polym. Sci.* **1999**, *74*, 2439.
(12) Labelle, C. B.; Gleason, K. K. *J. Appl. Polym. Sci.* **2001**, *80*, 2084.
(13) Capps, N. E.; Mackie, N. M.; Fisher, E. R. *J. Appl. Phys.* **1998**, *84*, 4736.
(14) Park, C. K.; Kim, H. T.; Lee, C. H.; Lee, N. E.; Mok, H. *Microelectron. Eng.* **2008**, *85*, 375.
(15) d'Agostino, R.; Cramarossa, F.; Fracassi, F. In *Plasma Deposition, Treatment, and Etching of Fluorocarbons*; d'Agostino, R., Ed.; Academic Press: San Diego, CA, 1990; p 95.
(16) Martin, I. T.; Malkov, G. S.; Fisher, E. R. *J. Vac. Sci. Technol. A* **2004**, *22*, 227.
(17) Limb, S. J.; Labelle, C. B.; Gleason, K. K. *Appl. Phys. Lett.* **1996**, *68*, 2810.
(18) Yasuda, H.; Hsu, T. *J. Polym. Sci., Polym. Chem. Ed.* **1997**, *15*, 81.
(19) Haupt, M.; Barz, J.; Oehr, C. *Plasma Process. Polym.* **2008**, *5*, 33.
(20) Milella, A.; Palumbo, F.; Favia, P.; Cicala, G.; d'Agostino, R. *Plasma Process. Polym.* **2004**, *1*, 164.
(21) Magane, M.; Itabashi, N.; Nishiwaki, N.; Goto, T.; Yamada, C.; Hirora, E. *Jpn. J. Appl. Phys., Part 2* **1990**, *29*, L829.
(22) Schwarzenbach, W.; Tserepi, A.; Derouard, J.; Sadeghi, N. *Jpn. J. Appl. Phys., Part 1* **1997**, *36*, 4644.
(23) Kikosaka, Y.; Toyoda, H.; Sugai, H. *Jpn. J. Appl. Phys., Part 2* **1993**, *32*, L353.
(24) Booth, J. P.; Hancock, G.; Perry, N. D.; Toogood, M. *J. Appl. Phys.* **1989**, *66*, 5251.
(25) Suzuki, C.; Sasaki, K.; Kadota, K. *J. Appl. Phys.* **1997**, *82*, 5321.
(26) Liu, D.; Martin, I. T.; Fisher, E. R. *Chem. Phys. Lett.* **2006**, *430*, 113.
(27) Liu, D.; Martin, I. T.; Zhou, J.; Fisher, E. R. *Pure Appl. Chem.* **2006**, *78*, 1187.
(28) Martin, I. T.; Zhou, J.; Fisher, E. R. *J. Appl. Phys.* **2006**, *100*, 013301.
(29) McCurdy, P. R.; Bogart, K. H. A.; Dalleska, N. F.; Fisher, E. R. *Rev. Sci. Instrum.* **1997**, *68*, 1684.
(30) Bogart, K. H. A.; Cushing, J. P.; Fisher, E. R. *J. Phys. Chem. B* **1997**, *101*, 10016.
(31) Williams, K. L.; Fisher, E. R. *J. Vac. Sci. Technol. A* **2003**, *21*, 1688.
(32) Williams, K. L.; Fisher, E. R. *J. Vac. Sci. Technol. A* **2003**, *21*, 1024.
(33) Williams, K. L.; Martin, I. T.; Fisher, E. R. *J. Am. Soc. Mass. Spectrom.* **2002**, *13*, 518.
(34) Fisher, E. R.; Ho, P.; Breiland, W. G.; Buss, R. J. *J. Phys. Chem.* **1992**, *96*, 9855.
(35) Fisher, E. R.; Ho, P.; Breiland, W. G.; Buss, R. J. *J. Phys. Chem.* **1993**, *97*, 10287.
(36) McCurdy, P. R.; Butoi, C. I.; Williams, K. L.; Fisher, E. R. *J. Phys. Chem. B* **1999**, *103*, 6919.
(37) Bogart, K. H. A.; Ramirez, S. K.; Gonzales, L. A.; Bogart, G. R.; Fisher, E. R. *J. Vac. Sci. Technol. A* **1998**, *16*, 3175.
(38) Trevino, K. J.; Fisher, E. R. *Plasma Process. Polym.* **2009**, in press.
(39) Ashfold, M. N. R.; Castano, F.; Hancock, G.; Ketley, G. W. *Chem. Phys. Lett.* **1980**, *73*, 421.
(40) Cicala, G.; Milella, A.; Palumbo, F.; Rossini, P.; Favia, P.; d'Agostino, R. *Macromolecules* **2002**, *35*, 8920.
(41) Teii, K.; Hori, M.; Goto, T. *J. Appl. Phys.* **2000**, *87*, 7185.
(42) Liu, D.; Fisher, E. R. *J. Vac. Sci. Technol. A* **2007**, *25*, 1519.
(43) Zhou, J.; Fisher, E. R. *J. Phys. Chem. B* **2006**, *110*, 21911.
(44) King, D. S.; Schenck, P. K.; Stephenson, J. C. *J. Mol. Spectrosc.* **1979**, *78*, 1.
(45) Kessels, W. M. M.; McCurdy, P. R.; Williams, K. L.; Barker, G. R.; Venturo, V. A.; Fisher, E. R. *J. Phys. Chem. B* **2002**, *106*, 2680.
(46) Butoi, C. I.; Mackie, N. M.; McCurdy, P. R.; Peers, J. R. D.; Fisher, E. R. *Plasmas Polym.* **1999**, *4*, 77.
(47) Mackie, N. M.; Venturo, V. A.; Fisher, E. R. *J. Phys. Chem. B* **1997**, *101*, 9425.
(48) Stillahn, J. M.; Trevino, K. J.; Fisher, E. R. *Ann. Rev. Anal. Chem.* **2008**, *1*, 261.
(49) Wakisaka, A.; Gaumet, J. J.; Shimizu, Y.; Tamori, Y. *J. Chem. Soc., Faraday Trans.* **1993**, *89*, 1001.
(50) Sasaki, K.; Wakasaki, T.; Matsui, S.; Kadota, K. *J. Appl. Phys.* **2006**, *91*, 4033.
(51) Benedikt, J.; Schram, D. C.; van de Sanden, M. C. M. *J. Phys. Chem. A* **2005**, *109*, 10153.
(52) Stillahn, J. M.; Fisher, E. R. *J. Phys. Chem. C* **2009**, *113*, 1963.
(53) Becker, K. H.; Brenig, H. H.; Tatarczyk, T. *Chem. Phys. Lett.* **1980**, *71*, 242.
(54) Becker, K. H.; Tatarczyk, T.; Radic-Peric, J. *Chem. Phys. Lett.* **1979**, *60*, 502.

AM900034X